

1 **Rac GTPase activating protein ARHGAP25 regulates leukocyte**
2 **transendothelial migration in mice**

3

4

5 Running title: ARHGAP25 regulates leukocyte migration

6

7

8 Roland Csépanyi-Kömi^{*,†,#}, Éva Wisniewski^{*,#}, Balázs Bartos^{*}, Petra Lévai^{*}, Tamás Németh^{*},
9 **Bernadett Balázs^{*}**, Angela R. M. Kurz[†], Susanne Bierschenk[†], Markus Sperandio^{†,§}, Erzsébet
10 Ligeti^{*,§}

11

12 ^{*} Department of Physiology, Semmelweis University, Budapest, Hungary

13 [†] Walter Brendel Center of Experimental Medicine, Ludwig-Maximilians Universität,
14 Munich, Germany

15 ^{#, §} these authors contributed equally

16

17

18

19

20 Corresponding author: Professor Erzsébet Ligeti

21

Department of Physiology, Semmelweis University

22

1094 Budapest, Tűzoltó u. 37-47., Hungary

23

Phone: +361 459 1500 ext. 60457; Fax: +361 266 7480

24

Email: ligeti.erszsebet@med.semmelweis-univ.hu

25 **Abstract**

26 ARHGAP25 is a Rac-specific GTPase activating protein that is expressed primarily in
27 hematopoietic cells. The involvement of ARHGAP25 in regulating the recruitment of
28 leukocytes to inflammatory sites was investigated in genetically modified mice. Using
29 intravital microscopy we show that *Arhgap25*-deficiency affects all steps of leukocyte
30 recruitment with a predominant enhancement of transendothelial migration of neutrophilic
31 granulocytes. **Increased transmigration of *Arhgap25*-deficient leukocytes is demonstrated in
32 inflamed cremaster muscle venules, in a peritonitis model, and in an *in vitro* chemotaxis
33 assay.** Using bone marrow chimeric mice lacking ARHGAP25 in the hematopoietic
34 compartment, we show that enhanced migration in the absence of ARHGAP25 is due to
35 defective leukocyte function. In search for potential mechanisms of ARHGAP25-regulated
36 migration of neutrophils, we detected an increase in the amount of active, GTP-bound Rac
37 and Rac-dependent cytoskeletal changes in the absence of ARHGAP25 suggesting a critical
38 role of ARHGAP25 in counterbalancing the Rac-activating effect of nucleotide exchange
39 factors. Taken together, using *Arhgap25*-deficient mice we identified ARHGAP25 as a
40 relevant negative regulator of leukocyte transendothelial migration.

41 **Introduction**

42 In inflammation, neutrophil recruitment to sites of injury is essential for the fast and effective
43 elimination of injurious agents. The first step of recruitment consists in the activation of
44 vascular endothelial cells, which leads to increased expression of several cell surface
45 molecules including selectins and integrin ligands (1, 2). These molecules are recognized by
46 circulating leukocytes enabling the stepwise recruitment and extravasation of leukocytes into
47 inflamed tissue. Capture to the inflamed endothelium is followed by rolling of leukocytes
48 along the endothelium. Both capture and rolling are mediated by endothelial selectins and
49 leukocyte expressed selectin ligands (3). During rolling, leukocytes get into intimate contact
50 with the endothelial surface which enables binding of endothelium-expressed chemokines to
51 their respective ligand on the leukocyte surface triggering firm arrest of leukocyte on the
52 endothelium. Thereafter, leukocytes begin to crawl along the vessel wall searching for an
53 appropriate exit point for transmigration into tissue (diapedesis) (2, 4, 5). Extravasated
54 leukocytes are directed by chemotactic agents to the pathogens to be eliminated (6). All these
55 different types of movements require a precise spatial and temporal organization of the actin
56 cytoskeleton (7-9). Although our knowledge on the involved receptors and signaling
57 pathways has increased tremendously in the last decade (10), differences in the molecular
58 organization of the actin cytoskeleton underlying the different types of movements are still
59 poorly understood.

60 Members of the Rac/Rho subfamily of small GTP-binding proteins are key regulators
61 of the actin cytoskeleton (11). Their prevalence in the active, GTP-bound state depends on the
62 balance between the three major regulatory proteins: guanine nucleotide exchange factors
63 (GEFs) that promote the active state, GTPase activating proteins (GAPs) that counteract it,
64 and guanine nucleotide dissociation inhibitors (GDI) that conserve the inactive state (12, 13).
65 In case of the Rac/Rho subfamily, the potential number of GEFs and GAPs expressed in a

66 specific cell is especially high (14). The majority of these GEFs and GAPs are large proteins
67 composed of several effector, interactive and regulatory domains that suggest multiple
68 functions (13, 14). In neutrophils, a specific involvement of certain GEFs has been
69 investigated for different neutrophil effector functions including chemotaxis and adhesion
70 (15-17). In contrast, similar data on potentially interacting GAPs are still scarce (18-20).

71 In a recent study, we have shown that ARHGAP25 is a Rac-specific GAP expressed
72 primarily in hematopoietic cells (21). We also demonstrated that ARHGAP25 serves as a
73 negative regulator of phagocytosis and related superoxide production (21, 22). The aim of the
74 present study was to reveal the role of ARHGAP25 in the complex process of leukocyte
75 recruitment during inflammation. We provide the first detailed description of the *Arhgap25*^{-/-}
76 mice, and show that loss of ARHGAP25 affects several steps along the recruitment cascade
77 leading to a proinflammatory phenotype with elevated transmigration of neutrophils into
78 inflamed tissue which is accompanied by increased Rac activity in neutrophils.

79 **Materials and Methods**

80 **Antibodies and reagents**

81 Anti-CD11b-PE and anti-Ly-6G-Pacific Blue were purchased from BioLegend, rat IgG2bκ-
82 PE isotype control and anti-CD18-FITC from BD Biosciences, rat IgG2a-APC isotype
83 control, anti-CD11a-APC, anti-human Fcγ-biotin, Streptavidin-PECy5 and rat IgG2a-FITC
84 isotype control from eBioscience, anti-CXCR2-APC, recombinant murine (rm) TNFα, rmE-
85 selectin/CD62E-Fc chimera and rmICAM-1/CD54-Fc chimera from R&D Systems,
86 rmKC/CXCL-1 and rmCXCL12 from PreproTech, Ly-6G-PerCP-Cy5.5 and CD11b-PE from
87 BD Pharmingen, mouse anti-Rac antibody from BD Transduction Laboratories,
88 paraformaldehyde from Sigma-Aldrich. Anti-human ARHGAP25 polyclonal antibody was
89 prepared as described previously.(21) Cross-reactivity with mouse ARHGAP25 was tested
90 using the lysate of COS-7 cells transfected with human *ARHGAP25-V5* and mouse *Arhgap25-*
91 *V5* constructs (see Fig. S1 for details). All other reagents were of research grade.

92
93 **Mice**

94 The *Arhgap25*^{-/-} mouse strain used for this research project was created from ES cell clone
95 (EPD0085_1_C10) obtained from the NCCR-NIH supported KOMP Repository
96 (www.komp.org) and generated by the CSD consortium for the NIH funded Knockout Mouse
97 Project (KOMP). Methods used on the CSD targeted alleles have been published in (23).
98 *Arhgap25*^{-/-} mice had a C57BL/6 genetic background and were maintained in a homozygous
99 breeding colony. Genotyping was performed according to KOMP's instructions using the
100 following primers: Common-loxP-F: 5'-GAGATGGCGCAACGCAATTAAT-3'; CSD-
101 *Arhgap25*-SR1: 5'-GCATGAGGCAGCTGTTCTTAGTTACC-3'; CSD-*Arhgap25*-GF4: 5'-
102 TGCACACGGTGGCATCTCTACTAAAG-3'. Analysis of blood parameters was carried out
103 with a haemocytometer. To reveal differences in body weight between wild type and

104 *Arhgap25*^{-/-} mice, 5-week-old animals (3 males/genotype and 2 females/genotype) were
105 weighed for 14 weeks. *Arhgap25*^{-/-} and control wild-type bone marrow chimeras were
106 generated using bone marrow cells from adult donors as described previously (24, 25).
107 *Arhgap25*^{-/-} bone marrow cell suspensions were injected intravenously into lethally irradiated
108 (11.5-Gy) recipients carrying the CD45.1 allele on the C57BL/6 genetic background. An
109 equal number of control chimeras were also generated using *Arhgap25*-expressing
110 (*Arhgap25*^{+/+}) bone marrow cells and will be referred to as wild-type chimeras. Efficiency of
111 repopulation of the hematopoietic compartment by donor-derived cells was more than 98%,
112 tested 4 weeks after transplantation by flow cytometry: we tested the expression of CD45.2
113 (donor) allele in the granulocyte gate determined by Ly-6G-staining, as described previously
114 (24, 25) (data not shown). Bone marrow chimeras were used 4-8 weeks after transplantation.
115 Mouse strain carrying the CD45.1 allele on the C57BL/6 genetic background (B6.SJL-Ptprca)
116 was purchased from The Jackson Laboratory (Bar Harbor, ME). Mice were kept in
117 individually sterile ventilated cages (Tecniplast, Buguggiate, Italy) in a conventional facility.
118 Age and gender-matched animals were used for all the experiments. Animal experiments were
119 approved by the Regierung von Oberbayern, Germany, AZ 55.2.1.54-2532-76-12, and by the
120 Governmental Office of Pest County, Hungary (22.1/S321/3/2011).

121

122 **Intravital microscopy of the mouse cremaster muscle**

123 Mice were pretreated with intrascrotal injection of 500 ng rmTNF α per mice. After 2 h, mice
124 were anesthetized and trachea and carotid artery were cannulated. Scrotum was opened, the
125 cremaster muscle exteriorized, spread over a cover glass and superfused with 35 °C
126 bicarbonate-buffered saline as described (26). Parameters of rolling, adhesion and crawling
127 were determined using an Olympus BX51WI intravital microscope equipped with a saline
128 immersion objective (40/0.8 NA, Olympus) and a CCD camera (model CF8/1, Kappa). All

129 scenes were recorded by the Virtual Dub software for later offline analysis. Systemic blood
130 samples (~ 50 μ L) were collected through the carotid artery catheter before and during the
131 experiment and analysed using a haemocytometer. The offline analysis of venular diameter
132 and vessel segment length of postcapillary venules (between 20-40 μ m in diameter) was
133 carried out with Fiji software (27). Leukocyte rolling flux fraction was calculated from the
134 number of rolling cells that crossed a perpendicular line through a given vessel within 1 min
135 in relation to the total number of circulating leukocytes (28). Velocities of rolling and
136 crawling were measured using MTrackJ plugin of Fiji software. Other experimental
137 parameters (centerline blood flow velocity, shear rate, systemic cell counts) are shown in
138 Table SI.

139

140 **TNF α -induced peritonitis model**

141 Mice were treated with intraperitoneal injection of 5 μ g rmTNF α in a final volume of 100 μ L.

142 Three hours after treatment, mice were sacrificed and peritoneal cavity was washed with 5 mL

143 ice-cold PBS supplemented with 20 mM HEPES and 10 mM EDTA. Ly-6G⁺ infiltrated cells

144 were analysed with BD FACSCalibur device. Cell counts were determined using Flow-Count

145 Fluorospheres (Beckman Coulter).

146

147 **Histology**

148 Three hours after intrascrotal injection of rmTNF α (500 ng in 200 μ L/mouse) or sterile PBS

149 (200 μ L/mouse), cremaster muscles were exteriorized, mounted on adhesive slides

150 (Superfrost, Thermo Scientific) and fixed in 4% (w/v) paraformaldehyde for at least 48 h at

151 4°C. Then samples were washed 3x5 min in 0.1 M Phosphate buffer (0.1 M NaH₂PO₄, 0.1 M

152 Na₂HPO₄ mixed in 81:19 ratio, pH 7.4) supplemented with 5% (v/v) ethanol and stained with

153 Giemsa's azure eosin methylene blue solution (Merck) for 4 min. After a rinse with water,

154 slices were differentiated with 0.03% (v/v) acetic acid for 10 min, and immersed in ascending
155 alcohol series from 70% (v/v) to absolute alcohol, in each for 3 min. Draining was carried out
156 with xylol (2x5 min), followed by sealing with rectangular coverslips using Eukitt (Sigma-
157 Aldrich). Whole mounts were analyzed with a Zeiss microscope equipped with an oil
158 immersion objective (100x/1.4 NA, Zeiss). Whole mounts of bone marrow chimeras were
159 analyzed with a Leica DMI 6000 B microscope equipped with an oil immersion objective
160 (63x/1.25 NA, Leica).

161 After 3 hours of TNF α challenge peritoneal tissue samples were taken and fixed in 4%
162 (w/v) phosphate-buffered paraformaldehyde for 48 hours. The tissue samples were paraffin-
163 processed, embedded, and 4 μ m sections cut with a Microm HM340E rotary microtome
164 (Thermo Fisher Scientific). Cut sections were then used for hematoxylin and eosin (H&E)
165 staining. Representative pictures were captured with a Nikon ECLIPSE Ni microscope
166 equipped with 10x/0.30 NA and 40x/0.75 NA dry objectives (Nikon) and a Nikon DS-Ri2
167 camera. Images were processed with NIS Elements v4.50 Imaging Software (Nikon).

168

169 **Ex vivo flow chamber assay**

170 Glass capillaries (Rectangular Boro Capillaries, 0.04x0.40mm, VitroCom) were coated
171 overnight with rmE-selectin (CD62E Fc chimera, 20 μ g/mL) or a combination of rmE-
172 selectin and rmICAM-1 (ICAM-1 Fc chimera, 15 μ g/mL) or a combination of rmE-selectin
173 and rmICAM-1 and rmKC/CXCL-1 (15 μ g/mL) at 4°C followed by blocking with 5% (w/v)
174 casein (Sigma-Aldrich) in PBS for 2h. Carotid artery catheter was connected directly to one
175 end of the chamber; while the other end was left open to regulate blood flow (shear stress
176 level was at 3-4 dyn/cm²). One representative field was recorded for 5 min using an Olympus
177 BX51WI intravital microscope equipped with a water immersion objective (40/0.8 NA,

178 Olympus) and a CCD camera (model CF8/1, Kappa). Rolling velocity was determined using
179 MTrackJ plugin of Fiji software.

180

181 **Transwell migration assay**

182 **In vitro migration of neutrophils was tested using a Transwell (Corning) assay with inserts of**
183 **3 µm pore size coated with 10% fetal bovine serum (FBS) for 1 hour at 37°C. Isolated cells**
184 **were pretreated with 50 µg/mL TNFα for 10 min in a 37°C incubator humidified with 5%**
185 **CO₂. For chemoattractant, 50ng/mL CXCL12 was used per well, containing 1x10⁶ cells. After**
186 **1 hour incubation at 37°C, transmigrated cells were counted using an acid phosphatase assay**
187 **(29).**

188

189 **Determination of leukocyte adhesion proteins and filamentous actin**

190 Neutrophils were isolated from bone marrow with percoll gradient centrifugation as described
191 previously (30). To determine cell surface expression of several receptors involved in
192 neutrophil migration, 100 µL whole blood was obtained retro-orbitally from wild type and
193 knock out mice pretreated with 500 ng TNFα intrascrotally for 2 h. **Alternatively,**
194 **transmigrated cells were collected from the Transwell plate. Then, whole blood or**
195 **transmigrated neutrophil samples were** transferred into 5 mL centrifuge tubes. Samples were
196 washed once with 3 mL HBSS⁺ medium (Hank's Balanced Salt Solution (Sigma-Aldrich)
197 supplemented with 1 mM CaCl₂, 1 mM MgCl₂, 0.1% (w/v) glucose, 10 mM HEPES and
198 0.25% (w/v) Bovine Serum Albumin (BSA), pH 7.4) and centrifuged with 350g for 5 min at
199 RT. Cells were stained with the indicated antibodies diluted in FACS buffer (PBS containing
200 1% (w/v) BSA), for 20 min at 4°C. After staining, 1 mL FACS Lysing Solution (BD
201 BioSciences) was added to the samples and cells were fixed on ice for 10 min. Then cells
202 were centrifuged with 350 g for 5 min at RT, resuspended in 300 µL FACS buffer and

203 analyzed by flow cytometry (Beckman Coulter Gallios). For actin-staining, 1×10^6 bone
204 marrow derived neutrophils were fixed with 4% (w/v) paraformaldehyde for 20 min at RT
205 and centrifuged with 500 g for 5 min at RT. Cells were permeabilized with 0.1% (v/v) Triton-
206 X-100 for 5 min at RT, then stained with Alexa-488-phalloidin (Life Technologies) in 1:500
207 dilution for 20 min at RT. Filamentous actin amount was analyzed with BD FACSCalibur
208 device. To investigate actin-polymerization in time, 1×10^6 bone marrow derived neutrophils
209 were stimulated with 50 ng/mL TNF α from 0 to 15 min at 37 °C. After stimulation, cells were
210 fixed and labelled with Alexa-488-phalloidin as detailed above.

211

212 **Soluble ICAM-1 binding assay**

213 For each sample, 1.5×10^6 cells were resuspended in 30 μ l HBSS⁺ and prewarmed at 37°C for
214 1 min. Pre-complexed master mix containing rmICAM-1-human Fc in 20 μ g/mL, anti-human
215 IgG1-biotin in 10 μ g/mL, Streptavidin-PE-Cy5 in 1:100 dilution and the indicated stimulus
216 were also prewarmed for 10 min at 37°C. Then, 10 μ L pre-complexed master mix was added
217 to 30 μ L cell suspension and incubated for 3 min at 37°C. Reaction was stopped with 900 μ L
218 ice-cold FACS Lysing Solution, samples were transferred on ice and fixed for 10 min. Cells
219 were washed with 2 mL HBSS⁺ and centrifuged with 350 g for 5 min at 4 °C. Then cells were
220 stained with anti-Ly-6G-Pacific Blue in 1:600 dilutions for 20 min at 4°C. After a washing
221 step (350 g, 5 min at 4°C in 2 mL HBSS⁺), cells were resuspended in 300 μ L HBSS⁺ and
222 analyzed by flow cytometry (Beckman CoulterGallios).

223

224 **Measurement of the amount of active Rac**

225 The cellular levels of GTP loaded Rac were determined with pull-down assay using GST
226 fusion proteins containing the GTPase-binding domain of p21-activated kinase (PAK) (GST-
227 PBD) as described (31, 32). GST-PBD has been expressed in *Escherichia coli*. For pull-down,

228 bone marrow-derived neutrophils were activated with 50 ng/mL TNF α in HBSS⁺ medium at
229 37 °C for 10 min. Basal Rac-activation was determined from resting cells. Whole cell lysates
230 were run on SDS-PAGE, blotted onto nitrocellulose (33) and stained with anti-Rac antibody
231 in 1:5000 dilution. Bound antibody was detected with enhanced chemiluminescence using
232 horseradish peroxidase-conjugated anti-mouse-Ig (from sheep) secondary antibody (GE
233 Healthcare) used in 1:5000 dilution. ImageJ software was used for densitometry analysis.

234

235 **Statistical analysis**

236 All data were analyzed and plotted using SigmaPlot 11.0 Software (Systat Software, Inc.).
237 Pairwise comparison of experimental groups was carried out with paired t-test or Mann-
238 Whitney Rank Sum Test or two way ANOVA followed by a Tukey post-hock test, depending
239 on the condition. All *P*-values<.05 were considered statistically significant.

240 **Results**

241

242 ***Arhgap25* knockout mice**

243 *Arhgap25* knockout mice were generated by the CSD consortium for the NIH funded
244 Knockout Mouse Project (KOMP) inserting the L1L2_Bact_P cassette upstream of the 6th
245 exon of the *Arhgap25* gene. The cassette contains the following sites and sequences in the
246 given order: FRT, lacZ, loxP, neomycin (under the control of the human beta-actin promoter),
247 SV40 polyA, FRT, loxP. A third loxP site was inserted downstream of the 6th exon (23).
248 Fertile homozygous mice (*Arhgap25*^{-/-}) were obtained with the expected Mendelian ratios
249 (data not shown) and did not show any obvious phenotype. No ARHGAP25 protein could be
250 detected in either bone marrow derived neutrophils or in the spleen of *Arhgap25*^{-/-} mice (Fig.
251 S1A, B). Blood panel (e.g. circulating cell counts, hematocrit, mean corpuscular hemoglobin,
252 mean corpuscular hemoglobin concentration) of *Arhgap25*^{-/-} mice did not differ from the wild
253 type (*Arhgap25*^{+/+}) (Table I, Table SII). We assessed the body weight of male and female
254 mice during a 130 days period and in 3 independent experiments. Body weight of male
255 *Arhgap25*^{-/-} mice was decreased compared to wild type but in the case of female mice, no
256 difference was observed (Fig. S2).

257

258 **Reduced leukocyte rolling velocity and prolonged crawling in the absence of** 259 **ARHGAP25**

260 Using intravital microscopy, we first investigated leukocyte rolling, adhesion and crawling in
261 TNF α -stimulated cremaster muscle venules of WT (*Arhgap25*^{+/+}) and *Arhgap25*^{-/-} mice *in*
262 *vivo*. Microvessel diameters, wall shear rates, centerline blood flow velocities and circulating
263 leukocyte counts were similar between wild type and *Arhgap25*^{-/-} mice (Table SI). While we
264 observed no difference in leukocyte rolling (Fig. 1A), mean leukocyte rolling velocity was

265 markedly decreased in the absence of ARHGAP25 (Fig. 1B). Furthermore, we analyzed the
266 number of adherent leukocytes and found no difference in adhesion between *Arhgap25*^{-/-} and
267 WT mice (Fig. 1C). Next, we investigated leukocyte crawling along the inflamed
268 endothelium. Individual crawling paths of >140 cells were analyzed per group (Fig. 1D and
269 E). We did not observe any difference in crawling directionality or accumulated distance
270 between WT and ARHGAP25^{-/-} mice (Fig. 1D-F). However, we found a significant increase in
271 crawling velocity and Euclidean distance in *Arhgap25*^{-/-} mice compared to WT mice (Fig. 1G
272 and H) suggesting that ARHGAP25 is regulating leukocyte crawling *in vivo*.

273

274 **Lack of ARHGAP25 augments transendothelial migration *in vivo*.**

275 Next, we studied leukocyte extravasation in TNF α -stimulated cremaster muscle whole mount
276 preparations of WT and *Arhgap25*^{-/-} mice. As shown in Fig. 2A-B, *Arhgap25*^{+/+} leukocytes
277 were found mainly in the vessels and the extravasated cells were scattered in the tissue. In
278 contrast, a large number of *Arhgap25*^{-/-} leukocytes lined up around the vessel from which they
279 extravasated (Fig. 2C-D). Transendothelial migration was quantified and we found a
280 significant increase in leukocyte extravasation in *Arhgap25*^{-/-} compared to WT mice (Fig. 2E).

281 **Intrascrotal injection of PBS as a control caused no significant difference between WT and**

282 ***Arhgap25*^{-/-} mice (P= 0.194, data not shown).** Further analysis of the different leukocyte

283 populations extravasated into the inflamed cremaster muscle tissue revealed that the major

284 component of extravasated leukocytes were neutrophilic granulocytes (PMN), followed by

285 monocytes and lymphocytes (marked as "Others") and eosinophils (Fig. 2F). **Increased**

286 **leukocyte extravasation upon TNF α stimulus was confirmed in an acute peritonitis model.**

287 **Analyzing the H&E stained sections of inflamed peritoneal tissue, elevated leukocyte**

288 **infiltration was observed in *Arhgap25*^{-/-} mice compared to WT (Fig. 3A). Specific analysis of**

289 Ly-6G⁺ neutrophil count in peritoneal lavage revealed a significant increase in case of
290 *Arhgap25*^{-/-} neutrophils compared to WT (Fig. 3B).

291

292 **Leukocyte rolling and adhesion under *ex vivo* conditions and *in vitro* Transwell**
293 **migration assay.**

294 As *Arhgap25*^{-/-} mice are complete knockout mice, the question arose, whether the observed
295 alterations are due to functional changes in leukocytes or endothelial cells. To investigate the
296 contribution of leukocytes on the recruitment phenotype observed in *Arhgap25*^{-/-} mice, we
297 performed *ex vivo* flow chamber assays and assessed rolling and adhesion of leukocytes in
298 flow chambers coated with adhesion relevant proteins. In flow chambers coated with
299 recombinant murine (rm)E-selectin, we saw a 2.5-fold increase in the number of rolling
300 *Arhgap25*^{-/-} leukocytes compared to wild type leukocytes (Fig. 4A). Next, we analyzed
301 leukocyte adhesion in flow chambers coated with rmE-selectin alone, with rmE-selectin and
302 rmICAM-1, and with rmE-selectin, rmICAM-1 and rmCXCL-1. Similar to the *in vivo* results
303 we found no difference in the number of adherent cells between the different groups (Fig.
304 4B). However, when we analyzed leukocyte rolling velocities, lack of ARHGAP25 resulted in
305 a significant decrease in rolling velocity (Fig. 4C) in flow chambers coated with rmE-selectin
306 or with rmE-selectin and rmICAM-1 surface (Fig. 4C).

307 Taken together, we were able to reproduce under *ex vivo* conditions the pattern of
308 rolling and adherence observed in ARHGAP25-deficient animals under *in vivo* conditions
309 suggesting that loss of ARHGAP25 in leukocytes accounts for the observed pro-inflammatory
310 phenotype.

311 **In order to test the role of ARHGAP25 in cell migration under *in vitro* conditions, we**
312 **determined neutrophil migration toward CXCL12 in a Transwell assay. As shown in Fig. 4D,**

313 *Arhgap25*^{-/-} neutrophils pretreated with TNF α for 10 min showed a significant increase in
314 transmigration compared to WT.

315

316 **Verification of altered leukocyte function in bone marrow chimeras**

317 In view of the decisive role of the adhesive surface provided *in vivo* by the endothelial cells
318 we wanted to verify our flow chamber data in bone marrow chimeric mice. These animals
319 express the CD45.1 allele and carry *Arhgap25*^{-/-} or *Arhgap25*^{+/+} hematopoietic cell
320 populations that express CD45.2. Using these animals, we investigated the extravasation of
321 leukocytes in cremaster muscle whole mounts after 3 h local stimulation with TNF α . CD45.2-
322 expressing *Arhgap25*^{-/-} leukocytes were able to transmigrate more efficiently in CD45.1-
323 expressing WT recipients than *Arhgap25*^{+/+} cells (Fig. 5A-D). Similar to the results presented
324 in Fig. 2, we found a threefold increase in leukocyte extravasation in chimeric mice with
325 *Arhgap25*^{-/-} hematopoietic cells compared to chimeric mice where WT hematopoietic cells
326 had been transferred (Fig. 5E). Similar to the results obtained in complete knock-out animals,
327 mainly neutrophilic granulocytes were responsible for the increase in extravasation followed
328 by mononuclear cells (marked as “Others”) and eosinophils (Fig. 5F).

329 These results substantiate that the alteration of leukocyte transendothelial migration
330 observed in the absence of ARHGAP25 is due to primary changes in the hematopoietic
331 compartment but not in endothelial or other non-hematopoietic cell compartment.

332

333 **Potential mechanism of altered leukocyte function**

334 To examine, whether ARHGAP25 has a regulatory role in the expression of adhesion relevant
335 molecules and signaling events during neutrophil recruitment, we investigated cell surface
336 expression and ligand binding ability of receptors and molecules involved in leukocyte-
337 endothelial cell interactions. As shown in Fig. 6A, ARHGAP25 deficiency did not affect the

338 expression of $\beta 2$ integrins (CD18, CD11a and CD11b), L-selectin (CD62L), PSGL-1,
339 chemokine receptor CXCR2 or CD44. *In vitro* analysis of adhesion molecule expression after
340 direct chemotactic migration of neutrophils did not reveal any difference between WT and
341 *Arhgap25*^{-/-} cells either (data not shown). Lack of ARHGAP25 also did not result in any
342 difference in rmICAM-1 binding to LFA-1 in resting cells. As stimulation of bone marrow-
343 derived neutrophils leads to integrin activation and increased ligand binding (34), we also
344 investigated binding of rmICAM-1 to neutrophils stimulated with CXCL1 or PMA.
345 Compared to unstimulated controls, PMA caused a significant increase in rmICAM-1 binding
346 to LFA-1 on both *Arhgap25*^{-/-} and wild type neutrophils. However, ARHGAP25-deficiency
347 did not influence rmICAM-1 binding to stimulated neutrophils. (Fig. 6B).

348 Our previous study indicated that ARHGAP25 has a regulatory role in neutrophilic
349 functions through its GAP activity on Rac1 (21). *In addition, our in vitro* studies demonstrate
350 that it has a GAP activity on Rac2 as well (data not shown). Therefore, we investigated the
351 presence of active Rac in bone marrow-derived neutrophils. Interestingly, we observed no
352 difference in Rac-activity between ARHGAP25^{-/-} and wild type cells in the resting state (Fig.
353 6C). In contrast, treatment of neutrophils with TNF α resulted in a marked decrease of active
354 Rac in the presence of ARHGAP25, while the lack of ARHGAP25 completely abolished this
355 alteration (Fig. 6C).

356 As Rac is known to be a key regulator of actin-polymerization during leukocyte
357 migration (35, 36), we measured filamentous actin (F-actin) in *Arhgap25*^{-/-} and wild type BM
358 neutrophils. In resting ARHGAP25-deficient cells, increased F-actin was observed compared
359 to wild type cells (Fig. 6D). Similar difference could be revealed upon stimulation with TNF α
360 (Fig. 6E). Taken together, we suggest that ARHGAP25 affects actin-polymerization and
361 depolymerization through its GTPase activating effect on Rac.

362 **Discussion**

363 The present study provides a detailed characterization of leukocyte recruitment during
364 inflammation *in vivo* in ARHGAP25-deficient mice. Alterations have been uncovered for
365 several steps along the recruitment cascade, indicating a role for the protein in those
366 processes. Most remarkable is the increase of transmigrating neutrophils **observed both in the**
367 **inflamed cremaster muscle and the inflamed peritoneal cavity**. No striking changes were
368 found in circulating leukocyte counts between wild type and *Arhgap25*^{-/-} animals excluding
369 differences in circulating leukocyte numbers for the observed alterations in leukocyte
370 recruitment in the absence of ARHGAP25.

371 Alteration of leukocyte migration may be the result of primary changes in circulating
372 leukocytes, the endothelial cells, or both. Based on the following observations, we believe that
373 in case of ARHGAP25-deficient animals, the altered migration is caused by leukocytes: i)
374 ARHGAP25 was shown to be expressed primarily in hematopoietic cells (21) ii) all the
375 trafficking alterations observed in living animals could be reproduced with isolated cells
376 under *ex vivo* **or in vitro** condition iii) the difference between the movements of *Arhgap25*^{+/+}
377 and *Arhgap25*^{-/-} cells was reproduced in bone marrow chimeric animals *in vivo*, where the
378 deficiency affected only the hematopoietic but not the endothelial or other peripheral cells.

379 In control experiments it was verified that ARHGAP25-deficiency had no influence on
380 the expression of the major leukocyte adhesive proteins and receptors or ligand binding of β 2
381 integrins. On the other hand, stimulation of neutrophils with TNF α resulted in a significant
382 decrease in measurable GTP-bound Rac which was abolished by absence of ARHGAP25. The
383 observed increase in the amount of filamentous actin indicates the biological relevance of
384 enhanced Rac activity (Fig. 6). Deficiency in various RacGEFs was reported to result in
385 decreased amount of GTP-bound Rac and a decrease in phagocyte migration (16, 37, 38), i.e.
386 changes opposite to our findings in animals lacking ARHGAP25. We thus ascribe the

387 alteration of leukocyte trafficking in ARHGAP25-deficient animals to cytoskeletal
388 reorganization due to elevation of RacGTP concentration. In human endothelial cells
389 (HUVECs), TNF α was shown to induce actin-rearrangement through activation of Rho family
390 small G-proteins (39) and several studies reported the role of TNF α in neutrophil priming and
391 its involvement in neutrophil effector functions and inside-out signaling (40-43). Our findings
392 strongly suggest that the leukocyte-specific RacGAP ARHGAP25 is a critical player in
393 TNF α -induced, Rac-mediated actin reorganization in neutrophils. Two recent reports provide
394 important information on its physiological role: ARHGAP25 was shown to be required for
395 actin depolymerization in the course of phagocytosis (21, 44), and it was demonstrated to
396 undergo significant changes in its phosphorylation pattern and GAP activity upon biological
397 stimulation (45). TNF α -initiated modulation of the phosphorylation pattern of ARHGAP25
398 with subsequent alterations of its GAP function may provide the link between the cytokine
399 effect and the actin cytoskeleton rearrangement.

400 Taken together, our data indicate that ARHGAP25 is a critical negative regulator of
401 Rac activity and leukocyte transmigration. This qualifies ARHGAP25 as an interesting drug
402 target in autoimmune disorders (e.g. rheumatoid arthritis and multiple sclerosis) where
403 leukocyte recruitment is unwanted.

404

405 **Acknowledgements**

406 The authors are indebted to Professor Attila Mócsai for helpful suggestions and critical
407 reading of the manuscript and to Ms. Regina Tóth-Kun and Nadine Schmidt for expert
408 technical assistance.

409

410

411

412 **Authorship contributions**

413 R. Csépanyi-Kömi and É. Wisniewski carried out the majority of experiments and prepared
414 writing of the manuscript; B. Bartos, P. Lévai, A. Kurz and S. Bierschenk carried out part of
415 the experiments; T. Németh carried out the bone marrow transplantation; B. Balázs carried
416 out the histology on murine peritoneums; M. Sperandio and E. Ligeti supervised, coordinated
417 and financed the experimental work and had a major role in writing of the manuscript.

418

419 **Disclosure of Conflict of Interest**

420 The authors have no conflict of interest to disclose.

421

For Peer Review. Do not distribute. Destroy after use.

422 References

- 423 1. Rao, R. M., L. Yang, G. Garcia-Cardena, and F. W. Luscinskas. 2007. Endothelial-dependent
424 mechanisms of leukocyte recruitment to the vascular wall. *Circ Res* 101: 234-247.
- 425 2. Ley, K., C. Laudanna, M. I. Cybulsky, and S. Nourshargh. 2007. Getting to the site of
426 inflammation: the leukocyte adhesion cascade updated. *Nat Rev Immunol* 7: 678-689.
- 427 3. McEver, R. P. 2002. Selectins: lectins that initiate cell adhesion under flow. *Curr Opin Cell Biol*
428 14: 581-586.
- 429 4. Luster, A. D., R. Alon, and U. H. von Andrian. 2005. Immune cell migration in inflammation:
430 present and future therapeutic targets. *Nat Immunol* 6: 1182-1190.
- 431 5. Zarbock, A., and K. Ley. 2009. Neutrophil adhesion and activation under flow.
432 *Microcirculation* 16: 31-42.
- 433 6. Borregaard, N. 2010. Neutrophils, from marrow to microbes. *Immunity* 33: 657-670.
- 434 7. Insall, R. H., and L. M. Machesky. 2009. Actin dynamics at the leading edge: from simple
435 machinery to complex networks. *Dev Cell* 17: 310-322.
- 436 8. Meyer, W. H., and T. H. Howard. 1987. Actin polymerization and its relationship to
437 locomotion and chemokinetic response in maturing human promyelocytic leukemia cells.
438 *Blood* 70: 363-367.
- 439 9. Vicente-Manzanares, M., and F. Sanchez-Madrid. 2004. Role of the cytoskeleton during
440 leukocyte responses. *Nat Rev Immunol* 4: 110-122.
- 441 10. Futosi, K., S. Fodor, and A. Mocsai. 2013. Neutrophil cell surface receptors and their
442 intracellular signal transduction pathways. *Int Immunopharmacol* 17: 638-650.
- 443 11. Hall, A. 1998. Rho GTPases and the actin cytoskeleton. *Science* 279: 509-514.
- 444 12. Csepanyi-Komi, R., M. Levay, and E. Ligeti. 2012. Rho/RacGAPs: embarras de richesse? *Small*
445 *GTPases* 3: 178-182.
- 446 13. Ligeti, E., S. Welti, and K. Scheffzek. 2012. Inhibition and termination of physiological
447 responses by GTPase activating proteins. *Physiol Rev* 92: 237-272.
- 448 14. Csepanyi-Komi, R., D. Safar, V. Grosz, Z. L. Tarjan, and E. Ligeti. 2013. In silico tissue-
449 distribution of human Rho family GTPase activating proteins. *Small GTPases* 4: 90-101.
- 450 15. Kunisaki, Y., A. Nishikimi, Y. Tanaka, R. Takii, M. Noda, A. Inayoshi, K. Watanabe, F.
451 Sanematsu, T. Sasazuki, T. Sasaki, and Y. Fukui. 2006. DOCK2 is a Rac activator that regulates
452 motility and polarity during neutrophil chemotaxis. *J Cell Biol* 174: 647-652.
- 453 16. Lawson, C. D., S. Donald, K. E. Anderson, D. T. Patton, and H. C. Welch. 2011. P-Rex1 and
454 Vav1 cooperate in the regulation of formyl-methionyl-leucyl-phenylalanine-dependent
455 neutrophil responses. *J Immunol* 186: 1467-1476.
- 456 17. Gakidis, M. A., X. Cullere, T. Olson, J. L. Wilsbacher, B. Zhang, S. L. Moores, K. Ley, W. Swat, T.
457 Mayadas, and J. S. Brugge. 2004. Vav GEFs are required for beta2 integrin-dependent
458 functions of neutrophils. *J Cell Biol* 166: 273-282.
- 459 18. Costa, C., G. Germena, E. L. Martin-Conte, I. Molineris, E. Bosco, S. Marengo, O. Azzolino, F.
460 Altruda, V. M. Ranieri, and E. Hirsch. 2011. The RacGAP ArhGAP15 is a master negative
461 regulator of neutrophil functions. *Blood* 118: 1099-1108.
- 462 19. Cho, Y. J., J. M. Cunnick, S. J. Yi, V. Kaartinen, J. Groffen, and N. Heisterkamp. 2007. Abr and
463 Bcr, two homologous Rac GTPase-activating proteins, control multiple cellular functions of
464 murine macrophages. *Mol Cell Biol* 27: 899-911.
- 465 20. Gambardella, L., K. E. Anderson, C. Nussbaum, A. Segonds-Pichon, T. Margarido, L. Norton, T.
466 Ludwig, M. Sperandio, P. T. Hawkins, L. Stephens, and S. Vermeren. 2011. The GTPase-
467 activating protein ARAP3 regulates chemotaxis and adhesion-dependent processes in
468 neutrophils. *Blood* 118: 1087-1098.
- 469 21. Csepanyi-Komi, R., G. Sirokmany, M. Geiszt, and E. Ligeti. 2012. ARHGAP25, a novel Rac
470 GTPase-activating protein, regulates phagocytosis in human neutrophilic granulocytes. *Blood*
471 119: 573-582.

- 472 22. Lorincz, A. M., G. Szarvas, S. M. Smith, and E. Ligeti. 2014. Role of Rac GTPase activating
473 proteins in regulation of NADPH oxidase in human neutrophils. *Free Radic Biol Med* 68: 65-
474 71.
- 475 23. Testa, G., J. Schaft, F. van der Hoeven, S. Glaser, K. Anastassiadis, Y. Zhang, T. Hermann, W.
476 Stremmel, and A. F. Stewart. 2004. A reliable lacZ expression reporter cassette for
477 multipurpose, knockout-first alleles. *Genesis* 38: 151-158.
- 478 24. Nemeth, T., K. Futosi, C. Hably, M. R. Brouns, S. M. Jakob, M. Kovacs, Z. Kertesz, B. Walzog, J.
479 Settleman, and A. Mocsai. 2010. Neutrophil functions and autoimmune arthritis in the
480 absence of p190RhoGAP: generation and analysis of a novel null mutation in mice. *J Immunol*
481 185: 3064-3075.
- 482 25. Kovacs, M., T. Nemeth, Z. Jakus, C. Sitaru, E. Simon, K. Futosi, B. Botz, Z. Helyes, C. A. Lowell,
483 and A. Mocsai. 2014. The Src family kinases Hck, Fgr, and Lyn are critical for the generation of
484 the in vivo inflammatory environment without a direct role in leukocyte recruitment. *J Exp*
485 *Med* 211: 1993-2011.
- 486 26. Frommhold, D., A. Ludwig, M. G. Bixel, A. Zarbock, I. Babushkina, M. Weissinger, S.
487 Cauwenberghs, L. G. Ellies, J. D. Marth, A. G. Beck-Sickinger, M. Sixt, B. Lange-Sperandio, A.
488 Zerneck, E. Brandt, C. Weber, D. Vestweber, K. Ley, and M. Sperandio. 2008.
489 Sialyltransferase ST3Gal-IV controls CXCR2-mediated firm leukocyte arrest during
490 inflammation. *J Exp Med* 205: 1435-1446.
- 491 27. Schindelin, J., I. Arganda-Carreras, E. Frise, V. Kaynig, M. Longair, T. Pietzsch, S. Preibisch, C.
492 Rueden, S. Saalfeld, B. Schmid, J. Y. Tinevez, D. J. White, V. Hartenstein, K. Eliceiri, P.
493 Tomancak, and A. Cardona. 2012. Fiji: an open-source platform for biological-image analysis.
494 *Nat Methods* 9: 676-682.
- 495 28. Sperandio, M., J. Pickard, S. Unnikrishnan, S. T. Acton, and K. Ley. 2006. Analysis of leukocyte
496 rolling in vivo and in vitro. *Methods Enzymol* 416: 346-371.
- 497 29. Mocsai, A., M. Zhou, F. Meng, V. L. Tybulewicz, and C. A. Lowell. 2002. Syk is required for
498 integrin signaling in neutrophils. *Immunity* 16: 547-558.
- 499 30. Mocsai, A., E. Ligeti, C. A. Lowell, and G. Berton. 1999. Adhesion-dependent degranulation of
500 neutrophils requires the Src family kinases Fgr and Hck. *J Immunol* 162: 1120-1126.
- 501 31. Ren, X. D., and M. A. Schwartz. 2000. Determination of GTP loading on Rho. *Methods*
502 *Enzymol* 325: 264-272.
- 503 32. Benard, V., and G. M. Bokoch. 2002. Assay of Cdc42, Rac, and Rho GTPase activation by
504 affinity methods. *Methods Enzymol* 345: 349-359.
- 505 33. Levay, M., B. Bartos, and E. Ligeti. 2013. p190RhoGAP has cellular RacGAP activity regulated
506 by a polybasic region. *Cell Signal* 25: 1388-1394.
- 507 34. Nishida, N., C. Xie, M. Shimaoka, Y. Cheng, T. Walz, and T. A. Springer. 2006. Activation of
508 leukocyte beta2 integrins by conversion from bent to extended conformations. *Immunity* 25:
509 583-594.
- 510 35. Lammermann, T., and R. N. Germain. 2014. The multiple faces of leukocyte interstitial
511 migration. *Semin Immunopathol* 36: 227-251.
- 512 36. Park, H., M. M. Chan, and B. M. Iritani. 2010. Hem-1: putting the "WAVE" into actin
513 polymerization during an immune response. *FEBS Lett* 584: 4923-4932.
- 514 37. Herter, J. M., J. Rossaint, H. Block, H. Welch, and A. Zarbock. 2013. Integrin activation by P-
515 Rex1 is required for selectin-mediated slow leukocyte rolling and intravascular crawling.
516 *Blood* 121: 2301-2310.
- 517 38. Watanabe, M., M. Terasawa, K. Miyano, T. Yanagihara, T. Uruno, F. Sanematsu, A. Nishikimi,
518 J. F. Cote, H. Sumimoto, and Y. Fukui. 2014. DOCK2 and DOCK5 act additively in neutrophils
519 to regulate chemotaxis, superoxide production, and extracellular trap formation. *J Immunol*
520 193: 5660-5667.
- 521 39. Wojciak-Stothard, B., A. Entwistle, R. Garg, and A. J. Ridley. 1998. Regulation of TNF-alpha-
522 induced reorganization of the actin cytoskeleton and cell-cell junctions by Rho, Rac, and
523 Cdc42 in human endothelial cells. *J Cell Physiol* 176: 150-165.

- 524 40. Elbim, C., S. Chollet-Martin, S. Bailly, J. Hakim, and M. A. Gougerot-Pocidaló. 1993. Priming of
525 polymorphonuclear neutrophils by tumor necrosis factor alpha in whole blood: identification
526 of two polymorphonuclear neutrophil subpopulations in response to formyl-peptides. *Blood*
527 82: 633-640.
- 528 41. Elbim, C., S. Bailly, S. Chollet-Martin, J. Hakim, and M. A. Gougerot-Pocidaló. 1994.
529 Differential priming effects of proinflammatory cytokines on human neutrophil oxidative
530 burst in response to bacterial N-formyl peptides. *Infect Immun* 62: 2195-2201.
- 531 42. Jablonska, E., M. Kiluk, W. Markiewicz, and J. Jablonski. 2002. Priming effects of GM-CSF, IFN-
532 gamma and TNF-alpha on human neutrophil inflammatory cytokine production. *Melanoma*
533 *Res* 12: 123-128.
- 534 43. Bouaouina, M., E. Blouin, L. Halbwachs-Mecarelli, P. Lesavre, and P. Rieu. 2004. TNF-induced
535 beta2 integrin activation involves Src kinases and a redox-regulated activation of p38 MAPK. *J*
536 *Immunol* 173: 1313-1320.
- 537 44. Schlam, D., R. D. Bagshaw, S. A. Freeman, R. F. Collins, T. Pawson, G. D. Fairn, and S.
538 Grinstein. 2015. Phosphoinositide 3-kinase enables phagocytosis of large particles by
539 terminating actin assembly through Rac/Cdc42 GTPase-activating proteins. *Nat Commun* 6:
540 8623.
- 541 45. Wang, L. D., S. B. Ficarro, J. N. Hutchinson, R. Csepanyi-Komi, P. T. Nguyen, E. Wisniewski, J.
542 Sullivan, O. Hofmann, E. Ligeti, J. A. Marto, and A. J. Wagers. 2016. Phosphoproteomic
543 profiling of mouse primary hematopoietic stem and progenitor cells reveals new regulators
544 of HSPC mobilization. *Blood*.
- 545
- 546

547 **Footnotes:** 1 Experimental work was financially supported by the Hungarian Research Fund
548 (OTKA K108382) to E.L., by the European Community's Seventh Framework Programme
549 [FP7] under grant agreement n°HEALTH-F4-2011-282095 to M.S. and by Deutsche
550 Forschungsgemeinschaft SFB914, project B1 to M.S.

For Peer Review. Do not distribute. Destroy after use.

551 **Figure legends**

552

553 **Fig.1. Measurement of leukocyte rolling and crawling in TNF α -stimulated mouse**

554 **cremaster muscle venules.** Intravital microscopy was conducted to investigate leukocyte

555 recruitment in the mouse cremaster muscle 2 hours after injection of rmTNF α (500 ng/mouse

556 intrascrotally). (A) Leukocyte rolling flux fraction (%) is presented as mean+SEM of 33

557 vessels from 10 wild type mice and 42 vessels of 12 *Arhgap25*^{-/-} mice. Mean rolling velocity

558 of leukocytes ($\mu\text{m/s}$) (B) was quantified and is shown as bar chart (mean+SEM of 166

559 *Arhgap25*^{+/+} cells and 190 *Arhgap25*^{-/-} cells), ***: $P < .001$ compared to *Arhgap25*^{+/+}. (C)

560 Number of adherent cells per mm^2 vessel wall is given as mean+SEM of 10 (*Arhgap25*^{+/+})

561 and 12 (*Arhgap25*^{-/-}) separate experiments. (D, E) Leukocyte crawling paths of individual

562 leukocytes of *Arhgap25*^{+/+} (n=163 cells) and *Arhgap25*^{-/-} (n=154 cells) mice. Direction of

563 blood flow is indicated by arrows. (F) Accumulated distance of leukocytes. Mean+ SEM of 8

564 wild type and 7 *Arhgap25*^{-/-} mice. (G) Mean crawling velocity presented as mean+SEM of

565 163 *Arhgap25*^{+/+} and 154 *Arhgap25*^{-/-} cells. **: $P < .01$ compared to *Arhgap25*^{+/+}. (H)

566 Euclidean distance determines the length of section between starting and end points of

567 crawling pathways. Mean+SEM of 8 (*Arhgap25*^{+/+}) and 7 (*Arhgap25*^{-/-}) separate experiments

568 are shown. *: $P < .05$ compared to *Arhgap25*^{+/+}.

569

570 **Fig. 2. Transmigration of leukocytes under *in vivo* conditions.** (A-D) Representative

571 images of Giemsa-stained cremaster muscle whole mounts from *Arhgap25*^{+/+} and *Arhgap25*^{-/-}

572 mice 3 hours after 500 ng intrascrotal rmTNF α injection. Images were captured with a Leica

573 DMI 6000 B microscope equipped with a 10x/0.30 NA dry objective (Leica) and a Leica DFC

574 480 camera. ROIs with high leukocyte infiltration (rectangles) are captured with 40x objective

575 and shown in the right side of the panel (B,D). Bars represent 100 μm . (E) Quantification of

576 total number of extravasated cells per mm² microvessel wall surface. (F) Distribution of
577 extravasated cell types (PMN: neutrophilic granulocytes, Eos: eosinophilic granulocytes,
578 Others: lymphocytes, macrophages and basophilic granulocytes). Mean+SEM of 3
579 (*Arhgap25^{+/+}*) and 7 (*Arhgap25^{-/-}*) separate experiments.***: *P* < .001 compared to
580 *Arhgap25^{+/+}*.

581

582 **Fig. 3. TNF α -induced leukocyte infiltration into the peritoneal cavity.**

583 (A) Hematoxylin and eosin staining of peritoneal tissues 3 hours after intraperitoneal injection
584 of TNF α . Left side of the panel indicates 2 representative images from *Arhgap25^{+/+}* and 2
585 from *Arhgap25^{-/-}* mice captured with a 10x objective. ROIs with high leukocyte infiltration
586 (rectangles) are captured with 40x objective and shown in the right side of the panel. Bars
587 represents 50 μ m. Results shown are representatives of multiple experiments and of multiple
588 sections and fields. (B) Ly-6G⁺ cell count measured from peritoneal lavage of *Arhgap25^{+/+}*
589 and *Arhgap25^{-/-}* mice 3 hours after TNF α administration. Data represent mean+SEM of 6
590 separate experiments. *: *P* < .05 compared to *Arhgap25^{+/+}*.

591

592 **Fig. 4. Leukocyte rolling and adhesion under flow conditions and transmigration in a**

593 **Transwell assay.** (A-C) *Ex vivo* flow chamber assay. Blood cells of *Arhgap25^{+/+}* and
594 *Arhgap25^{-/-}* mice were perfused through glass capillaries coated with different cell surface
595 molecules as indicated in panel B. Number of rolling (A) and adherent (B) leukocytes per
596 field of view (FOV) and mean rolling velocity (C) of wild type and *Arhgap25^{-/-}* animals are
597 shown. Rolling was assessed in E-selectin coated chambers (A). E: rmE-selectin; I: rmICAM-
598 1; CXCL1: rmKC/CXCL1. Mean+SEM of 4 separate experiments. *: *P* < .05, **: *P* < .01, ***:
599 *P* < .001 compared to *Arhgap25^{+/+}*. (D) *In vitro* transmigration of *Arhgap25^{+/+}* and *Arhgap25^{-/-}*
600 bone marrow neutrophils pretreated with TNF α toward CXCL12 in an FBS-coated Transwell

601 system. Data represent mean+SEM of 4 independent experiments. *: $P < .05$ compared to
602 *Arhgap25*^{+/+}.

603

604 **Fig. 5. Leukocyte transmigration in bone marrow chimeric mice carrying *Arhgap25*^{-/-} or**
605 ***Arhgap25*^{+/+} hematopoietic cells.** (A-D) Representative images of a Giemsa-stained
606 cremaster muscle whole mount. Microscopic analysis was performed 3 hours after 500 ng
607 intrascrotal rmTNF α injection. Images were captured with a Leica DMI 6000 B microscope
608 equipped with a 10x/0.30 NA dry objective (Leica) and a Leica DFC 480 camera. ROIs with
609 high leukocyte infiltration (rectangles) are captured with 40x objective and shown in the right
610 side of the panel (B,D). Bars represent 100 μm . (E) Quantification of total number of
611 extravasated cells per mm^2 microvessel wall surface. (F) Distribution of transmigrated cell
612 types (PMN: neutrophilic granulocytes, Eos: eosinophilic granulocytes, Others: lymphocytes,
613 macrophages, basophilic granulocytes). Mean+SEM of 3 separate experiments. *: $P < .05$
614 compared to *Arhgap25*^{+/+}.

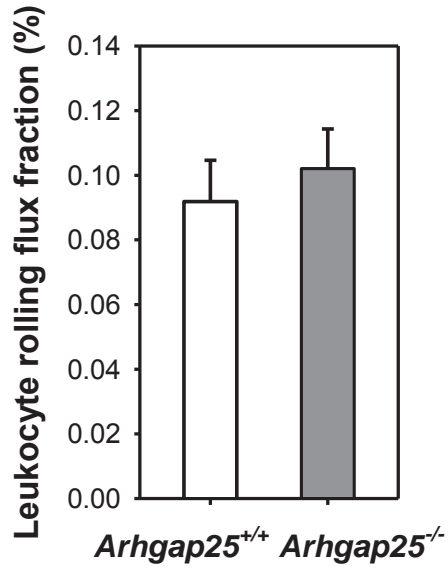
615

616 **Fig. 6. Investigation of the potential mechanism of altered migration in *Arhgap25*^{-/-} cells.**
617 (A) Cell surface expression of molecules relevant in leukocyte-endothelial cell interactions
618 during recruitment. Mean fluorescence intensity relative to isotype control is presented.
619 Mean+SEM of 5 separate experiments. Panel B shows binding of ICAM-1 to LFA1. Bone
620 marrow-derived neutrophils were co-incubated with fluorescently labeled rmICAM-1. Bound
621 ICAM-1 was detected with flow cytometry. Data are presented as mean fluorescence intensity
622 ratio relative to unstimulated cells. CCXL1: rmKC/CXCL1, PMA: Phorbol 12-myristate 13-
623 acetate. Mean+SEM of 4 separate experiments is shown. *: $P < .05$, **: $P < .01$. (C) GTP-
624 bound active Rac amount in resting and stimulated bone marrow-derived neutrophils.
625 Stimulation was carried out with 50 ng/mL TNF α in HBSS⁺ medium at 37 $^{\circ}\text{C}$ for 10 min.

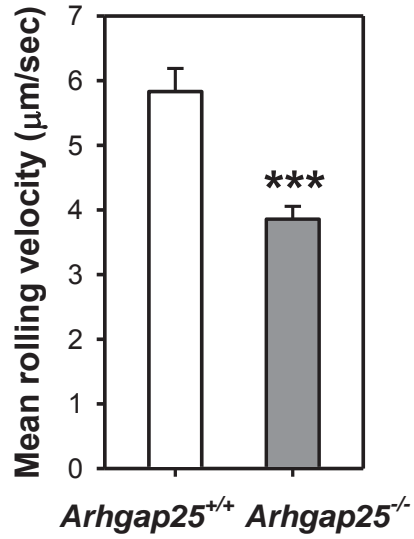
626 After lysis, active Rac was pulled down with PBD-GST-glutathione-sepharose beads. Bar
627 chart presents densitometric analysis of 6 (unstimulated) and 3 (TNF α -treated) separate
628 western blot experiments. Under the graph, a representative western blot experiment is shown.
629 Active and total Rac were decorated with anti-Rac antibody in 1:1000 dilution. (D, E)
630 Filamentous actin amount of bone marrow-derived neutrophils. Actin was stained with Alexa-
631 488-Phalloidin in 1:500 dilution and measured with flow cytometry. Pane D shows F-actin
632 content in resting neutrophils from *Arhgap25*^{-/-} mice as mean fluorescence intensity of
633 phalloidin relative to *Arhgap25*^{+/+}. Mean \pm SEM of 4 separate experiments is present. **: $P <$
634 .01 compared to *Arhgap25*^{+/+}. (E) Changes in relative F-actin content of neutrophils treated
635 for 5, 10 and 15 minutes with 50 ng/mL TNF α . Mean fluorescence intensity of phalloidin is
636 expressed relative to unstimulated (0 min) control in each genotype. Mean \pm SEM of 6 separate
637 experiments is shown. *: $P <$.05 compared to *Arhgap25*^{+/+}.

Figure 1.

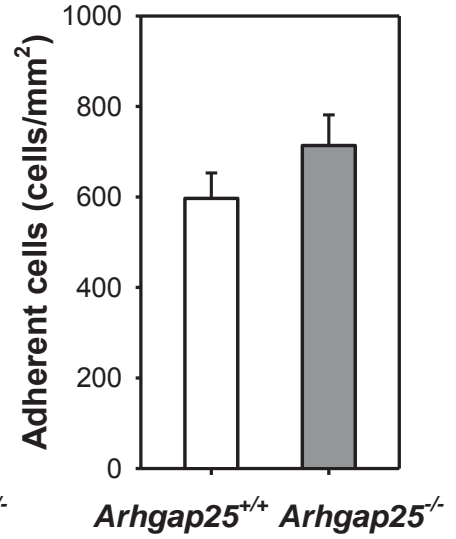
A



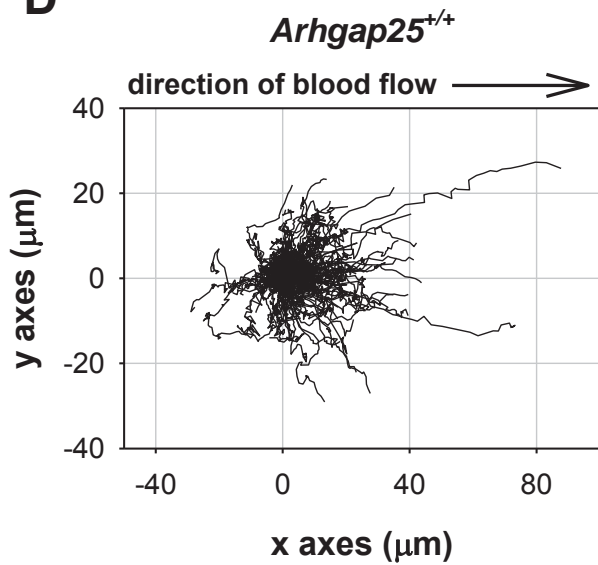
B



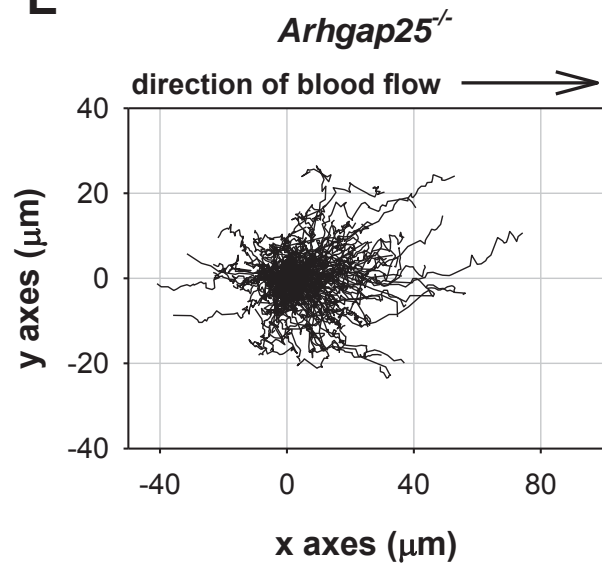
C



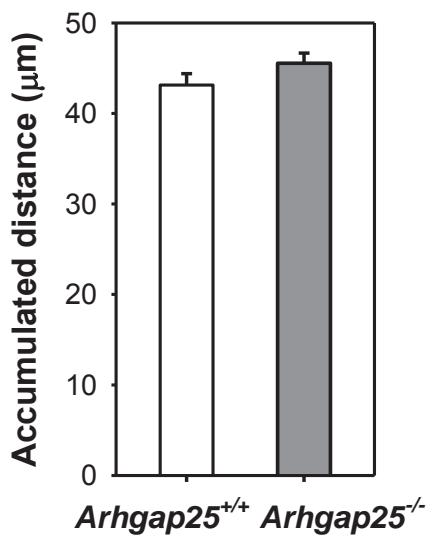
D



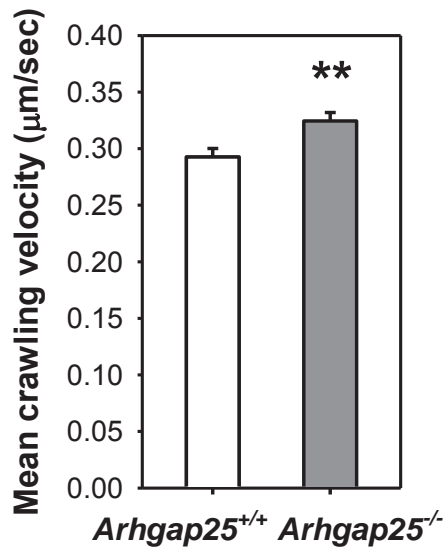
E



F



G



H

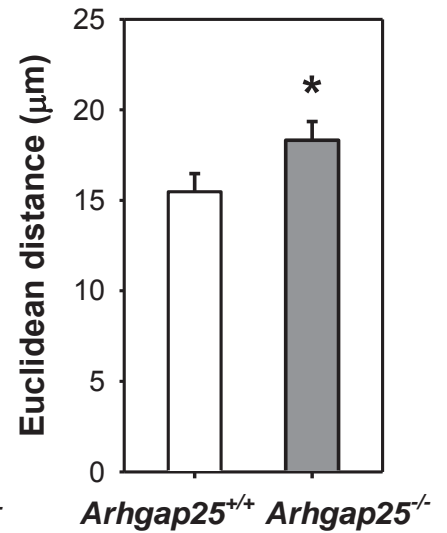


Figure 2.

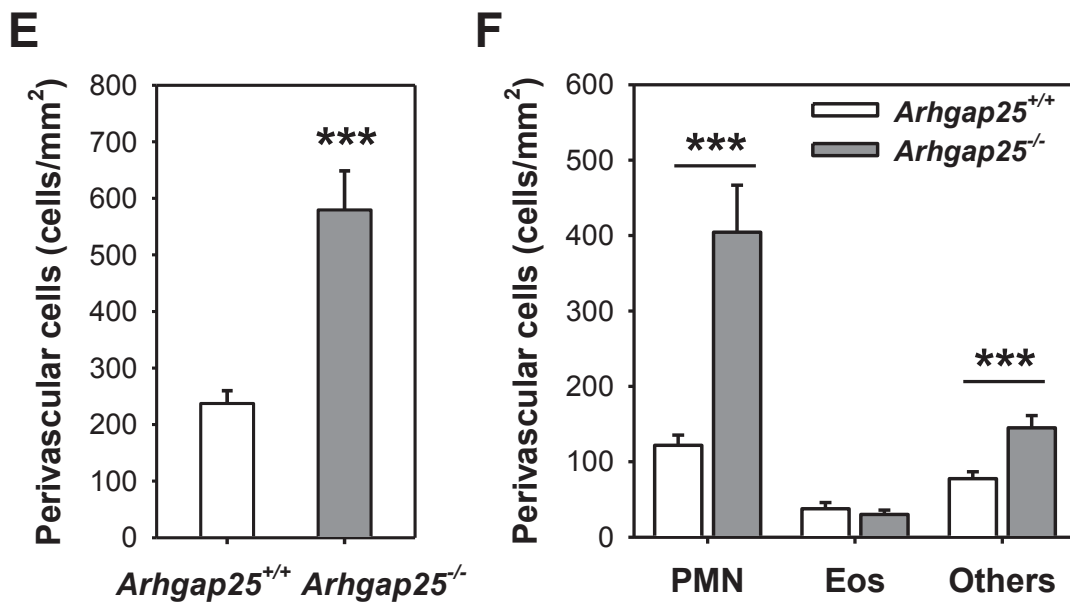
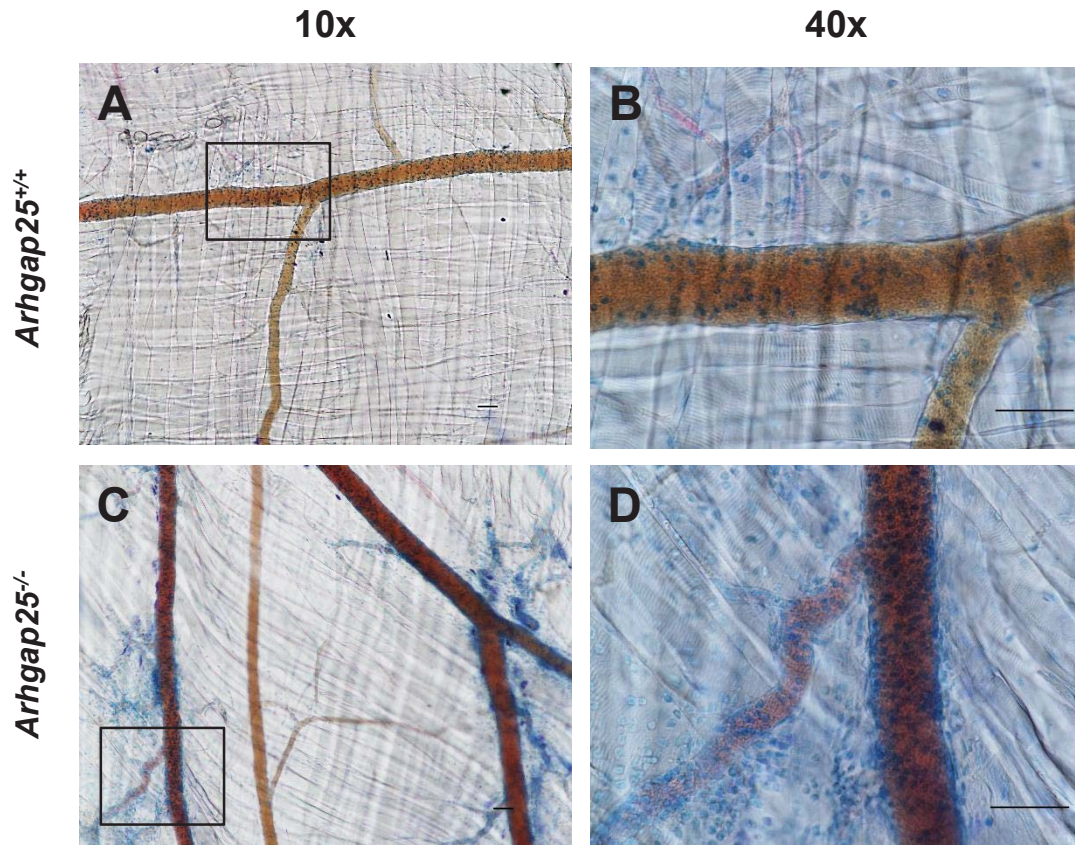


Figure 3.

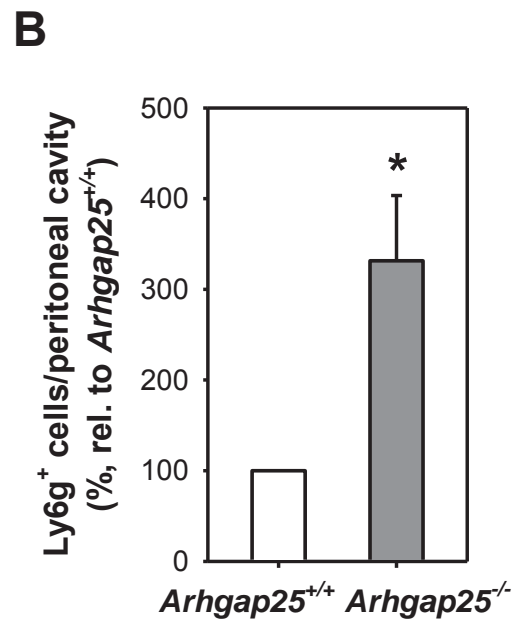
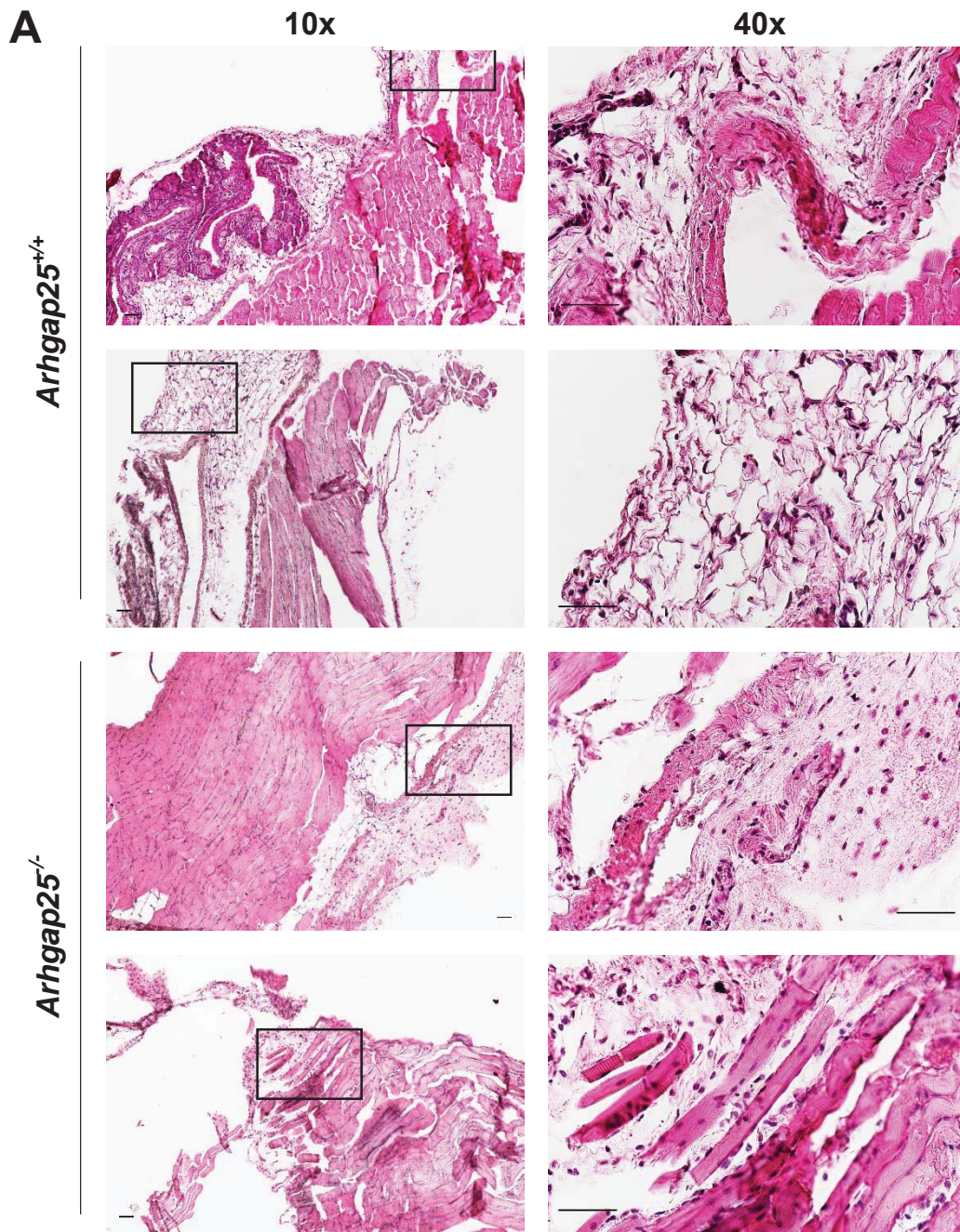


Figure 4.

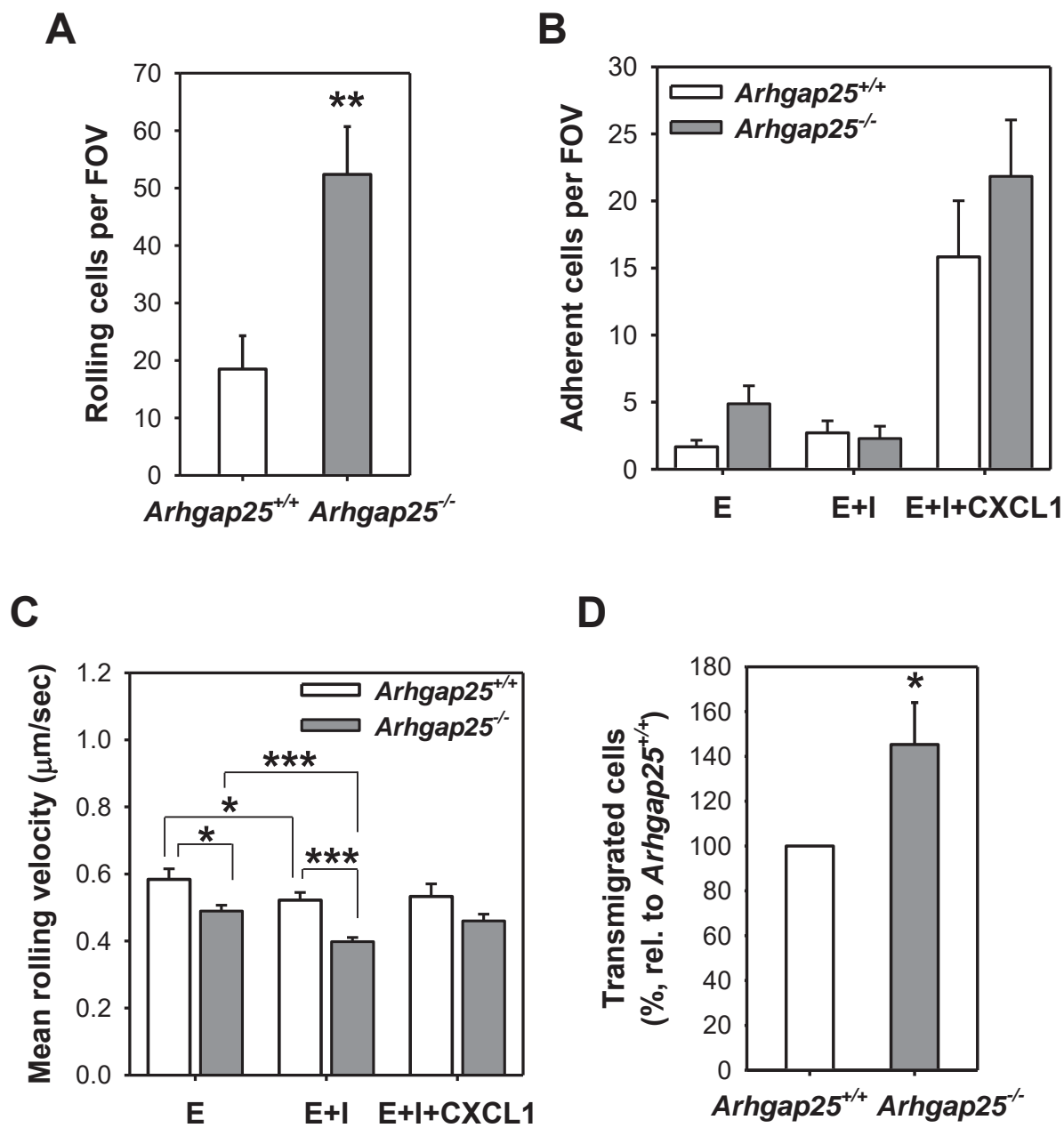


Figure 5.

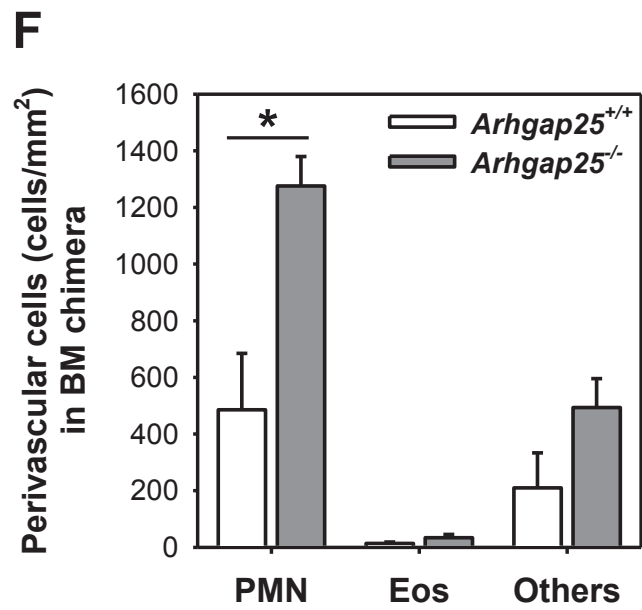
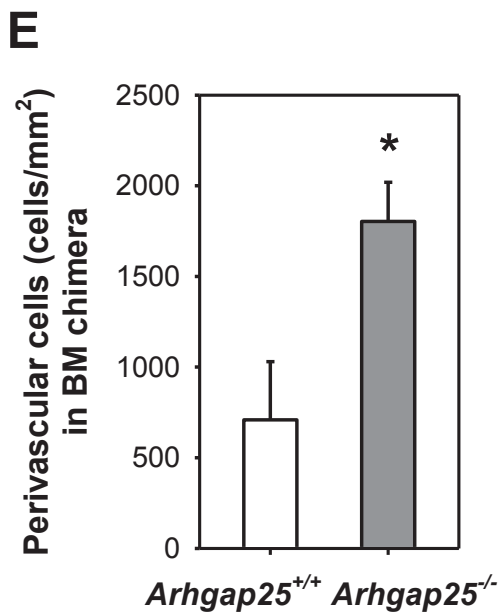
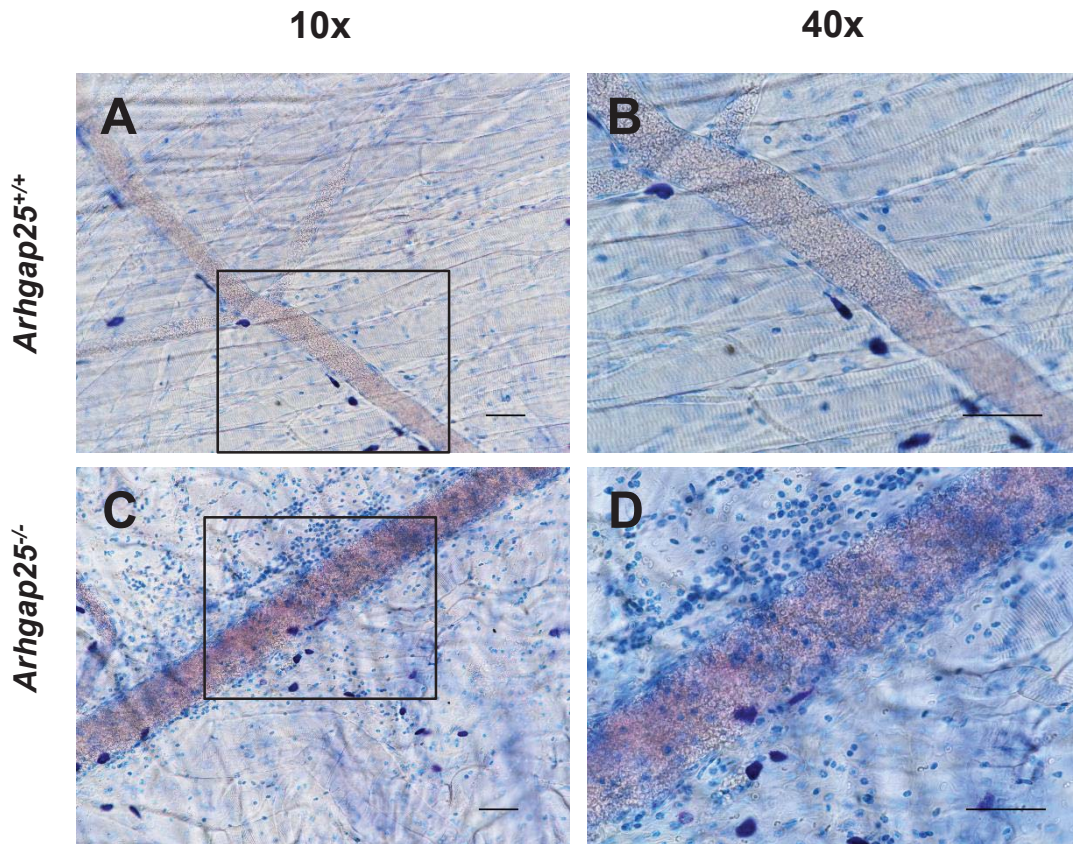
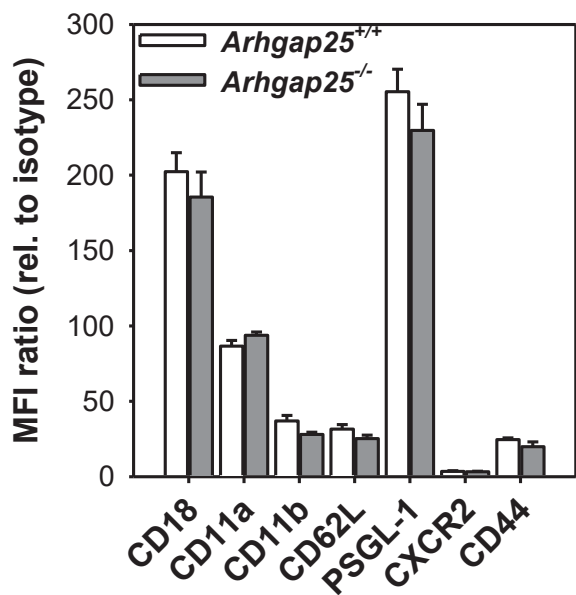
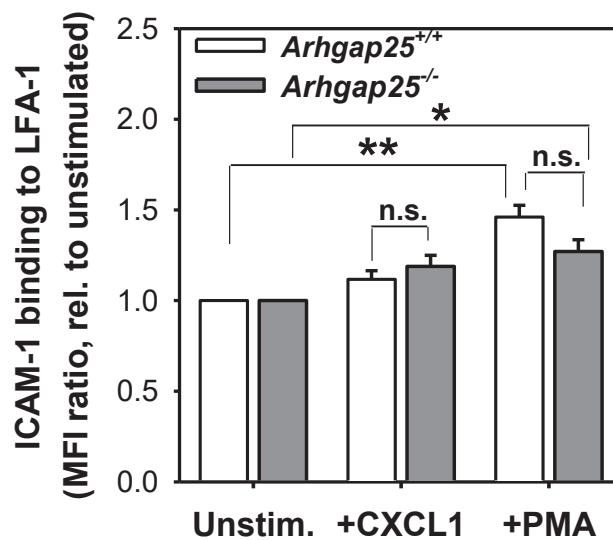


Figure 6.

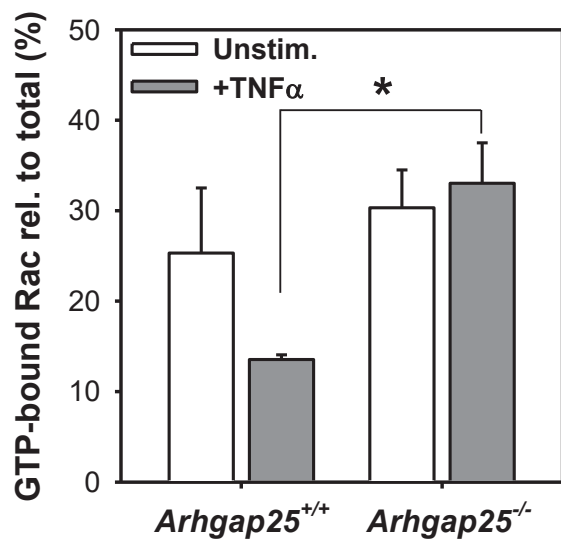
A



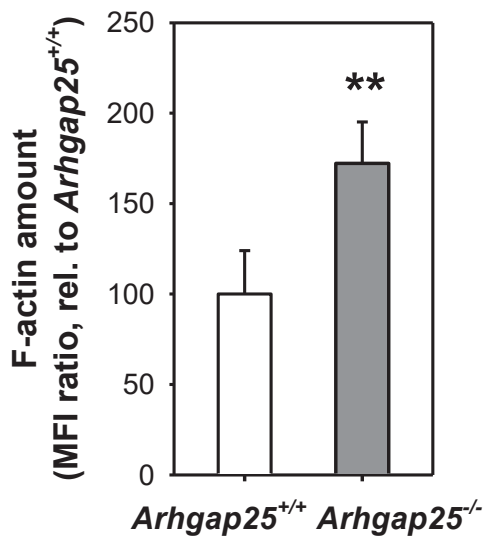
B



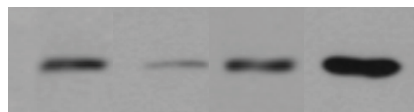
C



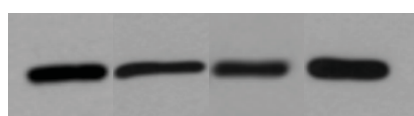
D



Active Rac



Total Rac



TNF α

- + - +

E

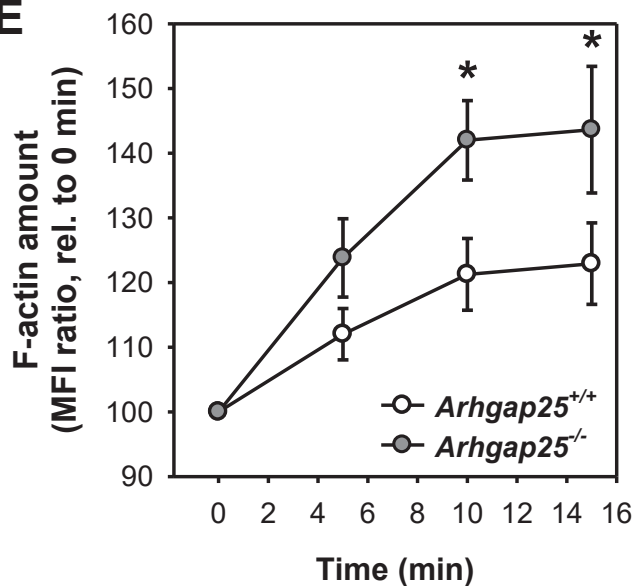


Table I. Blood parameters in *Arhgap25*^{+/+} and *Arhgap25*^{-/-} mice.

Parameter	<i>Arhgap25</i> ^{+/+}	<i>Arhgap25</i> ^{-/-}
Red blood cells, 10 ⁶ /uL	10.75 ± 0.08	10.69 ± 0.22
Hematocrit, %	52.78 ± 0.6	53.58 ± 1.57
MCH, pg	14.83 ± 0.06	14.55 ± 0.03
MCHC, g/dL	30.23 ± 0.14	29.05 ± 0.27
Reticulocytes, 10 ³ /μL	421.53 ± 32.01	469.35 ± 12.73
Platelets, 10 ³ /μL	807.00 ± 11.88	1017.25 ± 53.07
WBCs, 10 ³ /μL	5.72 ± 1.17	6.11 ± 0.59
Neutrophils, 10 ³ /μL	2.06 ± 0.27	2.32 ± 0.38
Lymphocytes, 10 ³ /μL	3.54 ± 1.20	3.60 ± 0.49
Monocytes, 10 ³ /μL	0.013 ± 0.005	0.085 ± 0.035
Eosinophils, 10 ³ /μL	0.103 ± 0.020	0.093 ± 0.011
Basophils, 10 ³ /μL	0.005 ± 0.003	0.008 ± 0.003

Data presented as mean ± SEM, n= 4 in each genotype. WBCs: white blood cells, MCH: mean corpuscular hemoglobin, MCHC: mean corpuscular hemoglobin concentration.